Formation of Medium-Heavy Elements in Rapid Neutron Capture Process

M. IKRAM[1,*], S. K. SINGH[2] AND S. K. PATRA[2]

[1]Department of Physics, Aligarh Muslim University, Aligarh-202002, India

[2]Institute of Physics, Sachivalaya Marg, Bhubaneswar-751005, India.

*Email: ikram@iopb.res.in

Abstract: We predict the neutron drip-line and simulate the r—process path for Cu — Sn, based on the calculation of binding energy in the frame-work of relativistic and non-relativistic mean field formalisms. We also compare the quadrupole deformation parameter β_2, and one neutron separation energy S_n of these isotopic series with the results of finite range droplet model (FRDM) prediction. The results produced by RMF and SHF are comparable to each other and also agreeable with the FRDM model.

1. INTRODUCTION

The elements available in nature are generally formed by the thermonuclear fusion process, up to Fe, Co or Ni. After the formation of Fe or Co, direct fusion process becomes endothermic, and the isotopes beyond Fe are formed by rapid neutron capture process (r—process). Approximately half of the heavier nuclei beyond Fe are formed in nature by this process [1-3]. Basically two types of neutron capture processes occur for astrophysical nucleosynthesis, which have been first identified by Burbidge et al. [1] and Cameron et al. [2]. The neutron capture processes which are based on neutron flux are characterised by rapid- and slow-processes. The r—process, which occurs at large neutron density, enables the production of neutron-rich nuclei close to the drip-line, while the s—process has sufficient time for beta disintegration and produces the nuclei near β-stability line. However, the production of medium-heavy elements (in particular Sr, Y and Zr) are more complex as it uses several mode of synthesis. The r—process requires such physical condition in which there are high entropy, fast expansion or low

Ikram, M.
Singh, S.K.
Patra, S.K.

electron fraction which is achieved after core collapse supernovae [4-7], but these physical conditions are still not well identified [8-11]. The r—process is able to determine the dynamics of astrophysical events due to the existence of unstable nuclei with very large exotic neutron-to-proton ratios [12]. After the successful exposure of nucleus to intense neutron flux, it undergoes β^-—decay to form stable nucleus. Even in the presence of intense neutron flux, a nucleus with a fixed Z can capture the neutron until the one neutron separation energy (S_n) falls to zero or negative ($S_n \leq 0$), which marks the neutron drip-line. Nuclei beyond the neutron drip-line decay by spontaneous neutron emission. Thus the neutron drip-line plays an important role for nucleosynthesis.

It is to assume that the formation of heavy elements takes the victory over the β^-—decay but it is not the end of whole story while the truth is a bit more complicated. The astrophysical events which maintain a very high temperature may have a possibility of photo-disintegration against the neutron capture because of significant role of gamma radiation flux. These gamma rays interact with the nuclei to break off the most loosely bound protons, neutrons, or alpha particles. The gamma photons literally break apart nuclei to form lighter elements. But instantly they are recaptured by other nuclei which binds them more tightly. So it might be a competition for neutron capture against photo-disintegration to form heavier nuclei. In such extreme environment, the time scale of the β—decay τ_β is much longer than the time of r—process or photo-disintegration. The two reverse (r—capture and photo-disintegration) reactions $n + (Z,N) \Leftrightarrow (Z,N+1) + \gamma$ can come to an equilibrium balance in course of time. The final product depends on several variables, most important of them are temperature, neutron flux density and β^-— decay. The β^-— decay $(Z,N) \rightarrow (Z+1,N-1) + \beta^- + \nu_e$ transfers a nucleus to the next higher Z number and determines the speed of formation of heavy nuclei [3]. The other factor which influence the r—process path is the high neutrino flux released in a supernovae explosion which has the same effect as β^-— decay $[\nu_e + (Z,N) \rightarrow (Z+1,N-1) + e^-]$ [3,9]. It is important to mention that the nuclear fission and also the α—decay do not occur for nuclei near the drip-line [13, 14] and may not be a factor in the way of r—process. In the present work, our aim is to determine the neutron drip-line and r—process path for $Cu — Sn$.

In the present work, we use the well established relativistic mean field (RMF) and non-relativistic Skyrme Hartree-Fock (SHF) approaches to study the neutron drip-line and rapid neutron capture process. The results are compared with the prediction of macro-microscopic finite range droplet model (FRDM) [15, 16]. For this, we evaluate the one neutron separation energy S_n to locate

the drip-line of the elements. Subsequently, we also evaluate the quadrupole deformation parameter β_2 and neutron skin thickness $\Delta r = r_n - r_p$ (r_n and r_p are the neutron and proton distribution radii) to see the structure effect of the drip-line nuclei. The paper starts with a short introduction in Sec. 1. The formalism of RMF and SHF theories are presented in Sec.2. Results and discussions are given in Sec. 3. Section 4 contains a summary of the paper.

2. THE MATHEMATICAL DETAILS OF FORMALISMS

A. Relativistic mean field formalism

From last three decades, the RMF theory is applied successfully to study the structural properties of nuclei throughout the periodic table [17-19] starting from the proton drip-line to the neutron drip-line. The starting point of the RMF theory is the basic Lagrangian containing Dirac spinors interacting with the meson fields [17-20]

$$
\begin{aligned}
\mathcal{L} =\ & \bar{\psi}_i \left\{ i\gamma^\mu \partial_\mu - M \right\} \psi_i + \frac{1}{2} \partial^\mu \sigma \partial_\mu \sigma - \frac{1}{2} m_\sigma^2 \sigma^2 - \frac{1}{3} g_2 \sigma^3 \\
& - \frac{1}{4} g_3 \sigma^4 - g_s \bar{\psi}_i \psi_i \sigma - \frac{1}{4} \Omega^{\mu\nu} \Omega_{\mu\nu} + \frac{1}{2} m_w^2 V^\mu V_\mu \\
& - g_w \bar{\psi}_i \gamma^\mu \psi_i V_\mu - \frac{1}{4} \vec{B}^{\mu\nu} \vec{B}_{\mu\nu} + \frac{1}{2} m_\rho^2 \vec{R}^\mu \vec{R}_\mu - \frac{1}{4} F^{\mu\nu} F_{\mu\nu} \\
& - g_\rho \bar{\psi}_i \gamma^\mu \vec{\tau} \psi_i \vec{R}^\mu - e \bar{\psi}_i \gamma^\mu \frac{(1 - \tau_{3i})}{2} \psi_i A_\mu.
\end{aligned}
\tag{1}
$$

Here m_σ, m_ω and m_ρ are the masses for nucleon, $\sigma-, \omega-$ and ρ-mesons and ψ is its Dirac spinor. Nucleons interact with the $\sigma, \omega,$, and ρ mesons. The field for the σ-meson is denoted by σ, ω-meson by V_μ and ρ-meson by R_μ. Electromagnetic interaction is denoted by A_μ field. g_s, g_ω, g_ρ and $e^4/\pi = 1/137$ are the coupling constants for the σ, ω, ρ-mesons and photon respectively. g_2 and g_3 are the nonlinear coupling constants for σ mesons. By using the classical variational principle we obtain the field equations for the nucleons and mesons. We use the recently reported NL3* parameter set [21]. This set of parameter reproduces both the ground and excited states properties of many spherical as well deformed nuclei [21]. The present coupled equations are solved self-consistently [19] in an axially deformed harmonic oscillator basis with 12 shells, both for bosons as well as Fermions. To take care of the pairing interaction, the

Ikram, M.
Singh, S.K.
Patra, S.K.

standard constant gap BCS - pairing approach is used [19] and the centre of mass energy is included with the formula $E_{c.m.} = (-3/4)41A^{-1/3}$ [19].

B. Non-relativistic Skyrme Hartree-Fock Hamiltonian density

The general form of the Skyrme effective interaction is used in the mean-field models, which is expressed as a density functional $\mathcal{H}$ [22, 23] given by some of the empirical parameters, as

$$\mathcal{H} = \mathcal{K} + \mathcal{H}_0 + \mathcal{H}_3 + \mathcal{H}_{eff} \cdots\cdots, \tag{2}$$

where $K, H_0 H_3$ and H_{eff} are the kinetic energy, zero range, density dependent and the effective mass dependent terms, respectively. These parameters can be written as;

$$\mathcal{H}_0 = \frac{1}{4}t_0[(2+x_0)\rho^2 - (2x_0+1)(\rho_p^2 + \rho_n^2)], \tag{3}$$

$$\mathcal{H}_3 = \frac{1}{24}t_3[(2+x_3)\rho^2 - (2x_3+1)(\rho_p^2 + \rho_n^2)] \tag{4}$$

and

$$\mathcal{H}_3 = \frac{1}{8}[t_1(2+x_1) + t_2(2+x_2)\tau\rho + \frac{1}{8}[t_2(2x_2+1)$$
$$-t_1(2x_1+1)](\tau_p\rho_p + \tau_n\rho_n). \tag{5}$$

The kinetic energy $K = \frac{\hbar^2}{2m}\tau$, is a form used in the Fermi gas model for non-interacting Fermions. The other terms representing the surface contributions of finite nucleus with b_4 and b_4' as additional parameters are

$$\mathcal{H}_{s\rho} = \frac{1}{16}\left[3t_1\left(1+\frac{1}{2}x_1\right) - t_2\left(1+\frac{1}{2}x_2\right)\right](\vec{\nabla}\rho)^2$$
$$-\frac{1}{16}\left[3t_1\left(x_1+\frac{1}{2}\right) - t_2\left(x_2+\frac{1}{2}\right)\right]$$
$$\times\left[\left(\vec{\nabla}\rho_n\right)^2 + (\vec{\nabla}\rho_p)^2\right] \tag{6}$$

and

$$\mathcal{H}_{s\vec{J}} = -\frac{1}{2}\left[b_4\rho\vec{\nabla}.\vec{J} + b_4'\left(\rho_n\vec{\nabla}.\vec{J}_n + \rho_p\vec{\nabla}.\vec{J}_p\right)\right], \tag{7}$$

where $\rho = \rho_n + \rho_p$ is the total nucleon density, the kinetic energy density $\tau = \tau_n + \tau_p$, and the spin-orbit density $\vec{J} = \vec{J}_n + \vec{J}_p$. Here n and p are the subscripts representing the neutron and proton, and m be the mass of nucleon. $\vec{J}_q = 0, q = n$ or p for spin saturated nuclei, i.e., for nuclei with major oscillator shells completely filled. The total binding energy of the nucleus is obtained by integrating the density function H [23, 24]. For the SHF calculation, the SkI4 set of Reinhard [24] is used which is designed for a better spin-orbit interaction. The BCS-δ interaction is adopted to take care of pairing in the open shell nuclei.

3. PARAMETRIZATION

As we have mentioned earlier, we also used the SkI4 parameter set for non-relativistic calculations. The values of binding energies obtained by this set is given in Table 1. One neutron separation energy S_n is also framed in this table. The agreeability of the calculated results with NL3, NL3* and FRDM can be seen from their comparison. The data of NL3 and NL3* are also presented in the Table 1. Although, the results of NL3* are claimed to be superior in Ref. [21], but here we find that the NL3 is still one of the best set among the relativistic forces. However, the one neutron separation energy S_n are comparable to each other along with the FRDM as well as experimental values. The considered nuclei are chosen in such a way that they lie in the range of our present study as well as experimentally known [25]. It is to notice that the final conclusion of our predictions for r—process path which is the main objective of the present study will remain unchanged. On the other hand, the drip-line which is very much sensitive to the binding energies may be differed from one to another by depending on the force parametrizations.

4. RESULTS AND DISCUSSIONS

A. Binding energy and quadrupole deformation parameter

We calculate the ground state binding energy and quadrupole deformation parameter for Z = 29 to 50 neutron-rich nuclei starting from the vicinity of neutron capture path till neutron drip-line. The results produced by RMF and SHF in the form of BE, β_2 and S_n are quite comparable with FRDM results [15, 16]. The drip-line nuclei are identified by the one neuron separation energy of two neighboring nuclei, which is expressed as

$$S_n(N,Z) = BE(N,Z) - BE(N-1,Z). \qquad (8)$$

The binding energy per nucleon (BE/A) for the drip-line nuclei of *Cu — Sn* is plotted in Fig. 1. It is noticed that the peak values of BE/A for Nb are at A =

Ikram, M.
Singh, S.K.
Patra, S.K.

Table 1: The ground state binding energy (MeV) and one neutron separation energy S_n (MeV) calculated by using NL3, NL3* and SkI4 parameter sets are given here. For better comparison, the FRDM as well as experimental binding energy and one neutron separation energy are also framed in this table.

Nuclei	RMF (NL3)		RMF (NL3*)		SHF (SkI4)		FRDM		Exp	&n
	BE	S_n	BE	S_n	BE	S_n	BE	S_n	BE	
^{76}Cu	644.112	5.290	641.820	5.050	642.570	4.521	642.25	4.34	641.710	4.580
^{81}Zn	676.695	2.820	673.770	2.870	672.846	3.314	677.07	2.15	676.510	2.620
^{83}Ga	695.341	3.620	692.660	3.620	691.025	3.742	694.83	4.15	694.920	4.400
^{85}Ge	713.537	3.790	710.960	3.760	708.996	3.720	713.50	2.48	714.150	3.050
^{87}As	731.191	3.980	728.910	4.010	727.319	4.183	731.52	5.00	732.010	4.730
^{90}Se	753.660	4.500	751.630	4.430	750.406	4.476	755.27	5.37	755.640	4.900
^{93}Br	775.054	3.880	773.060	3.820	771.965	3.798	776.08	5.07	776.180	4.770
^{97}Kr	800.722	3.890	797.880	3.910	797.327	3.762	803.86	3.01	802.180	2.420
^{99}Rb	820.099	3.940	817.510	4.010	815.496	3.935	822.72	5.09	821.320	4.960
^{102}Sr	843.385	4.090	840.750	3.980	836.849	3.098	841.95	3.25	845.910	4.870
^{103}y	857.398	4.510	854.820	4.390	851.110	3.710	860.18	5.40	859.290	5.360
^{105}Zr	875.491	4.920	872.840	4.790	869.973	5.118	878.69	3.68	877.670	3.810
^{109}Nb	903.759	4.900	900.830	4.740	900.121	5.454	905.94	5.58	904.260	5.090
^{ul}Mo	921.717	4.550	918.710	4.340	919.656	5.628	924.37	3.81	923.000	3.460
^{113}Tc	939.115	4.500	936.080	4.270	939.034	5.724	941.48	5.92	941.230	5.630
^{117}Ru	966.362	5.630	964.730	5.140	967.207	4.697	969.97	3.82	969.460	3.540
^{119}Rh	986.063	5.760	984.400	5.720	986.532	5.029	988.23	5.92	988.170	6.070
^{122}pd	1011.570	5.810	1009.580	5.680	1011.544	5.340	1013.55	6.31	1013.330	6.500
^{125}Ag	1037.138	5.790	1034.770	5.560	1036.771	5.294	1037.04	6.64	1036.380	6.100
^{128}Cd	1062.637	5.470	1059.790	5.160	1062.392	5.427	1063.87	6.93	1062.820	6.820
^{132}In	1092.831	2.510	1089.550	2.540	1090.941	1.888	1090.41	2.71	1089.490	2.460
^{135}Sn	1111.224	1.640	1108.140	1.680	1110.747	2.028	1111.52	1.87	1111.140	2.270

123, 124 in RMF, SHF and A = 133 for Ag in FRDM, respectively indicating the most stable drip-isotope of the series in the respective models. The quadrupole deformation parameter β_2 of drip-line nuclei are plotted in Fig. 2. We find the drip-line nuclei such as Br, Kr, Rb, Sr and Y with mass number A = 117, 118,
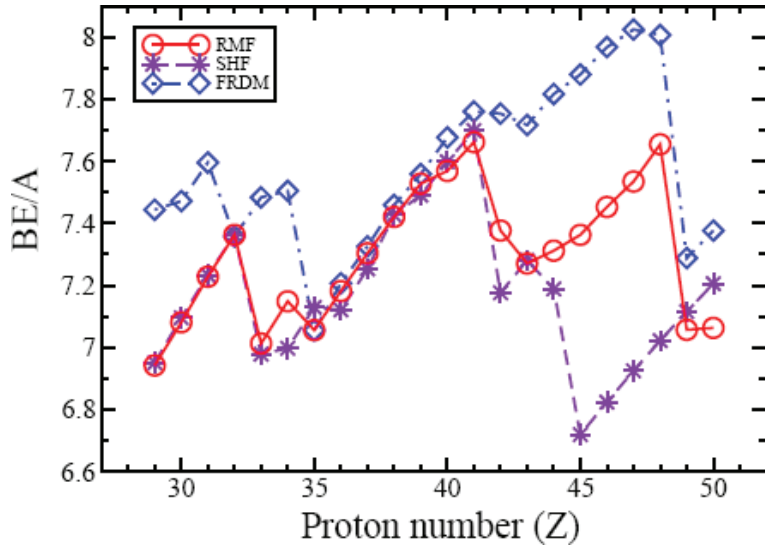
Figure 1: The binding energy per nucleon versus proton number Z for the neutron drip-line nuclei of *Cu — Sn* isotopic series.
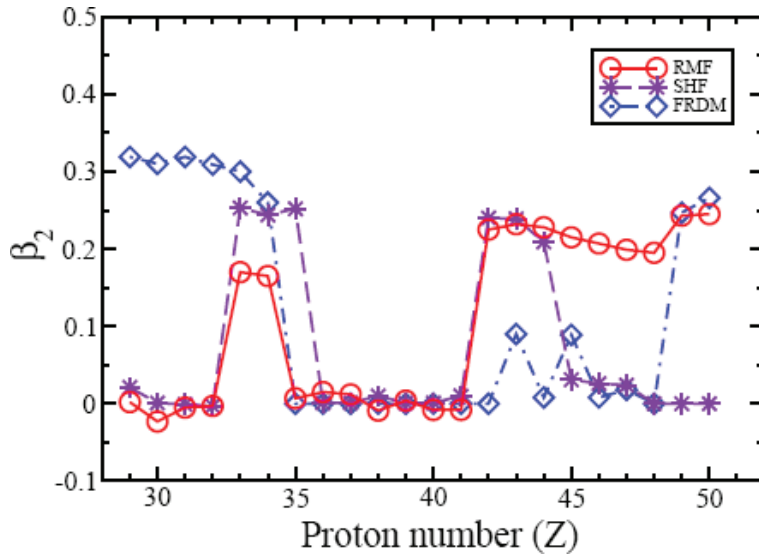

Figure 2: The ground state quadrupole deformation parameter β_2 as a function of proton number Z for neutron drip-line nuclei of *Cu — Sn* isotopic chain.

Ikram, M.
Singh, S.K.
Patra, S.K.

119, 120, 121 respectively have spherical shape in all the three models. Contrary to the spherical shape of ^{99}Cu in RMF and SHF, the FRDM gives a large prolate β_2 value. Note that ^{91}Cu and ^{91}Cu are the drip-line nuclei in the microscopic (RMF and SHF) and macro-micro (FRDM) models respectively (see Table II). The drip-line nuclei Zn, Ga and Ge with mass number 100, 101, 102 respectively have $\beta_2 \sim 0$ or mild oblate with RMF and SHF but FRDM gives large prolate shapes. The RMF and SHF predict prolate shape for ^{111}As and ^{112}Se drip nuclei. In contrast to the shape of these drip-line nuclei, FRDM gives a spherical shape for ^{103}As and ^{106}Se. From Fig. 2, it can also be seen that ^{123}Zr, ^{124}Nb and ^{122}Zr, ^{123}Nb are the drip-line nuclei in RMF and FRDM, respectively. These nuclei are predicted to be spherical in their ground state configuration. The drip-line nuclei from ^{132}Mo to ^{163}Sn in RMF have a prolate shape while there are prolate as well as spherical shapes in SHF and FRDM models.

B. Radii and neutron skin

The neutron and proton distributions inside the nucleus for these neutron-rich nuclei are quite informative to understand the nuclear equation of state at high

Table 2: The predicted neutron drip-line (d.l.) with RMF(NL3*) and SHF(SkI4) is compared with finite-range droplet model (FRDM)[13]. The range of the *r*—process of nucleosynthesis for *Cu — Sn* is also compared with FRDM[13].

| Nuclei	dripline			range			Nuclei	dripline			range		
	RMF	SHF	FRDM	RMF	SHF	FRDM		RMF	SHF	FRDM	RMF	SHF	FRDM
Cu	99	99	91	80-85	80-85	80-85	Zr	123	122	122	109-122	111-119	105-122
Zn	100	100	94	81-86	81-86	81-94	Nb	124	123	123	115-123	112-120	110-123
Ga	101	101	95	82-89	82-89	82-93	Mo	132	136	126	112-124	114-124	111-123
Ge	102	102	102	83-94	85-94	83-100	Tc	137	137	129	120-125	120-125	114-123
As	111	111	103	89-96	89-95	86-103	Ru	139	142	130	123-126	123-126	115-128
Se	112	114	106	91-97	91-100	87-104	Rh	141	157	131	125-127	126-127	124-129
Br	117	115	117	93-103	93-105	90-107	Pd	142	158	132	127-129	132-134	130-132
Kr	118	118	118	96-105	95-106	91-116	Ag	143	159	133	130-135	134-135	130-133
Rb	119	119	119	100-108	102-104	98-119	Cd	143	160	136	131-136	135-140	131-136
Sr	120	119	120	102-110	109-111	99-120	In	160	161	155	132-138	136-143	132-149
Y	121	121	121	107-121	110-121	102-121	Sn	163	162	156	133-148	133-147	133-152
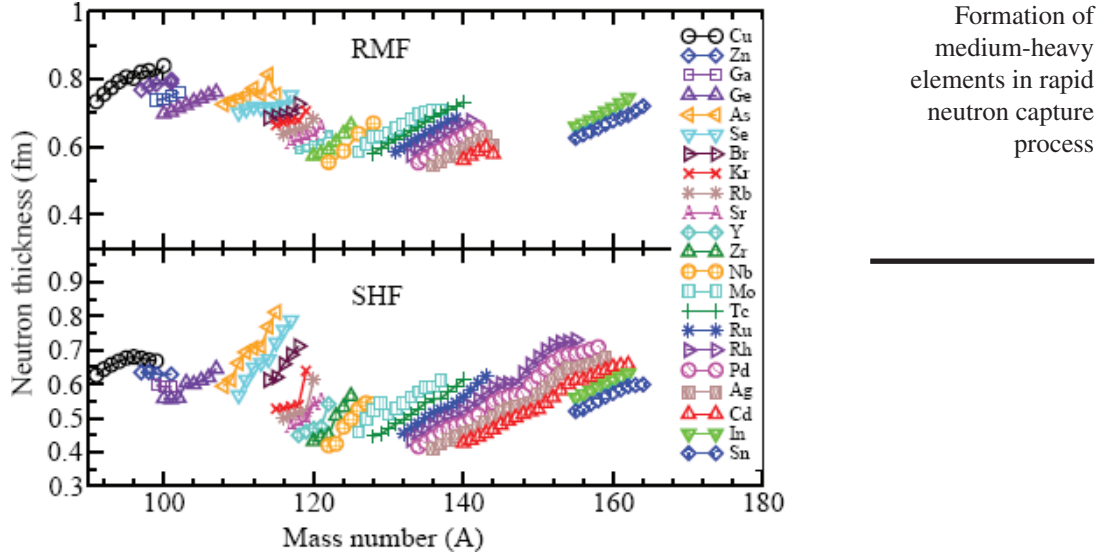
Figure 3: The calculated neutron skin thickness $\Delta r = r_n - r_p$ as a function of mass number A for exotic nuclei in *Cu — Sn* isotopic series.

neutron proton asymmetry. For this, we calculate the neutron (r_n) and proton (r_p) radii. The skin structure of nuclei are studied by taking the difference $\Delta r = r_n - r_p$, which is shown in Figure 3 for both RMF and SHF cases. We found large value of Δr in both the models. As expected, the distribution of neutrons is more extended inside the nucleus forming a skin like structure towards the tail region. The Δr values are found to be almost similar in both the formalisms. A further inspection reveals that the RMF predicts a slightly larger skin than the SHF. The typical ranges are, $\Delta r = 0.6 - 0.7$ fm and $0.5 — 0.6$ fm in RMF and SHF respectively.

C. Neutron drip-line and r-process path

The one neutron separation energy, S_n, which is an effective quantity for the determination of drip-line are plotted in Fig. 4 for all three models. On the basis of S_n, we determine the neutron drip-line. We have taken an uncertainty of 0.4 MeV in our calculation and defined the drip-line when S_n reaches to this value. The predicted neutron drip-lines are compared with the FRDM data in Fig. 5. It is evident from Fig. 5 that the predictions of drip-line by SHF and RMF are quite agreeable to each other. While the macro-microscopic prediction is quite different and reaches earlier than mean field predictions. As we have already mentioned, the drip-line is much sensitive and a function of binding energy. Variation in
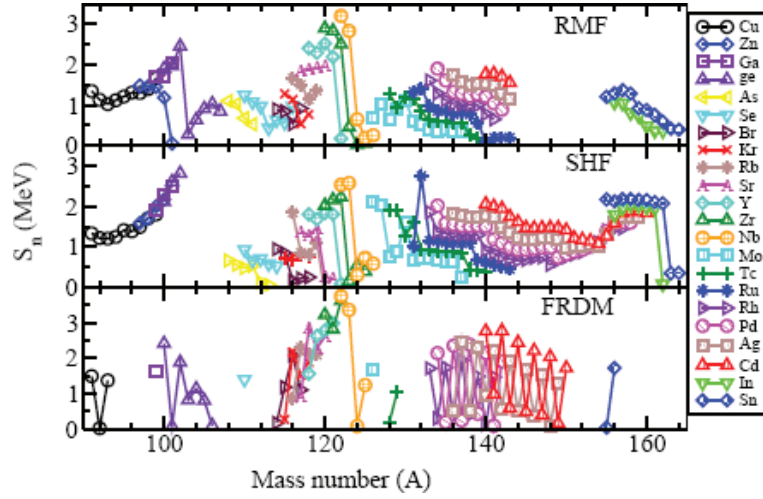
Ikram, M.
Singh, S.K.
Patra, S.K.

Figure 4: One neutron separation energy of of *Cu — Sn* isotopic chain with respect to mass number A.
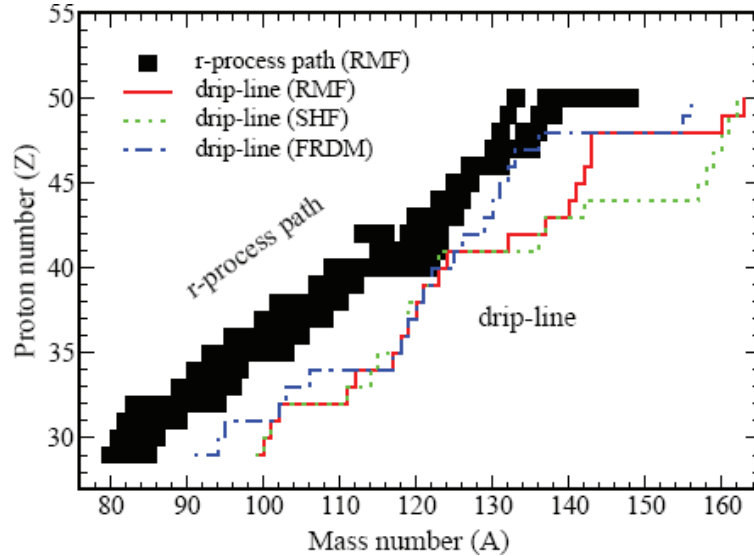

Figure 5: The rapid neutron capture process (*r—process*) path for the formation of *Cu — Sn* nuclei. The predicted neutron drip-line with RMF(NL3*) and SHF(SkI4) is compared with finite-range droplet model (FRDM) calculations. The S_n values of the black portion are within 2 — 4 MeV and considered to be the candidates for *r*—process at $T = 1 — 3 \times 10^9$K and neutron flux density $n_n = 10^{20-30}$ cm^{-3}.

binding energy calculated by different parameterizations or models affects the drip-line or more precisely, we can say it is model dependent. The dependency of model in prediction of neutron drip-line is reflected in our results.

A quantitative measurement of stability can be estimated by the neutron-to-proton ratio (N/Z) for the whole periodic chart. Larger the N/Z ratio, in general, lesser the stability against β—decay. The neutron-to-proton ratio for the band of nuclei having neutron separation energy within 2 — 4 MeV in RMF (NL3*) are shown in Figure 6. These nuclei are the possible candidates for the path of r—process, which are depicted by filled squares in Fig. 5. The N/Z values of these nuclei spread between ~1.6 — 2.0 and the most probable ratio is ~ 1.8 compare to the drip-line nuclei having the ratio ~2.3. This means, the nuclei belong to drip-line have more exotic nature than the participants of r—process.

The formation of heavy nucleus starting from Cu to Sn can be understood by rapid neutron capture process. Due to the presence of highly dense neutron flux, the normal nuclei Fe or Ni capture neutrons upto a maximum mass number and make one of the most neutron-rich nucleus having S_n ~ 2 – 4 MeV in the isotopic series. This ultra neutron-rich nucleus suffers a competition between the neutron capture process and β—decay. Ultimately, undergoes to β—emission and produces the less neutron-rich Cu nucleus. Again the Cu isotope captures neutrons till it reaches to $^{80-85}$Cu which lie much before the
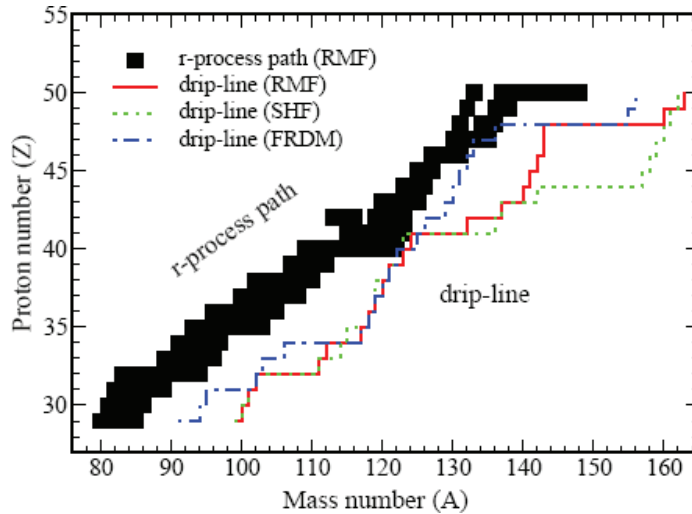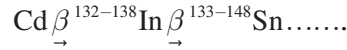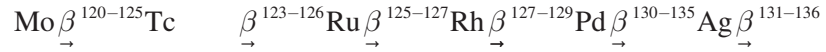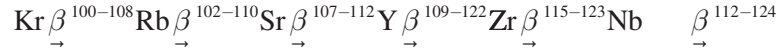

Figure 6: The neutron-to-proton ratio (N/Z) for drip-line nuclei in RMF(NL3*) and SHF(SkI4) are compared with FRDM predictions. The N/Z values for the r—process nuclei (S_n = 2 — 4 MeV) (denoted by *) are also shown.

Ikram, M.
Singh, S.K.
Patra, S.K.

neutron drip-line. Finally, attains the waiting point, emits the β—particle and formed the next heavier element Zn. This process continues and forms more and more heavier element as shown below:

Seed-nucleus(Fe-Ni)+n+ ....(waiting-point)

$\xrightarrow{\beta}{}^{80-85}Cu\xrightarrow{\beta}{}^{81-86}Zn\xrightarrow{\beta}{}^{82-89}Ga\xrightarrow{\beta}{}^{83-94}Ge\xrightarrow{\beta}{}^{89-96}As\xrightarrow{\beta}{}^{91-97}Se\xrightarrow{\beta}{}^{93-103}Br\xrightarrow{\beta}{}^{96-105}$

$Kr\xrightarrow{\beta}{}^{100-108}Rb\xrightarrow{\beta}{}^{102-110}Sr\xrightarrow{\beta}{}^{107-112}Y\xrightarrow{\beta}{}^{109-122}Zr\xrightarrow{\beta}{}^{115-123}Nb\qquad\xrightarrow{\beta}{}^{112-124}$

$Mo\xrightarrow{\beta}{}^{120-125}Tc\qquad\xrightarrow{\beta}{}^{123-126}Ru\xrightarrow{\beta}{}^{125-127}Rh\xrightarrow{\beta}{}^{127-129}Pd\xrightarrow{\beta}{}^{130-135}Ag\xrightarrow{\beta}{}^{131-136}$

$Cd\xrightarrow{\beta}{}^{132-138}In\xrightarrow{\beta}{}^{133-148}Sn\ldots\ldots$

It is obvious that the high temperature and neutron density belong to the favourable conditions to occur r—process. At temperature about $1 — 3 \times 10^9\,K$ and neutron flux $n_n = 10^{20} — 10^{30} cm^{-3}$ which is possible in a supernovae explosion and an ideal condition for the r—process, satisfies the relation [1, 26]:

$$Q_n = (10^9 / 5.04)[34.07 + 1.5\log 10^9 - \log n_n], \qquad (9)$$

where Q_n is the neutron binding obtained from S_n. While using the typical temperature and neutron flux in this relation, the likely value of Q_n lies within 2 to 4 MeV. It is shown in Ref. [27] that under neutron-rich environment and with favourable projectile energy, the formation of superheavy element in astrophysical object is possible by r—process.

We simulate the r—process path using these conditions of temperature and density range to the nuclei which also fulfill the S_n range from 2 to 4 MeV. The band of nuclei which participate to r—process are expressed in Table II. The r—process path unaffected as long as the S_n values lie between 2 —4 MeV. Our this observation agrees with the recent report of Lahiri and Gangopadhyay [28]. The abundance of neutron-rich nuclei in the r—process path in the way of the formation of heavier element lie much before the neutron drip-line as reflected in Fig. 5. In general, the range of nuclei contribute to r—process are in similar band (see Table II) and the drip-line predicted by RMF, SHF and FRDM are quite comparable with each other although there is a slight variation among them as shown in Fig. 5.

5. SUMMARY

As expected, the RMF and SHF produce quite successful results about the bulk properties of finite nuclei towards the drip-line. The calculated binding energies and quadrupole deformation parameters in RMF and SHF approaches

are found to be in close agreement with FRDM values for *Cu — Sn* isotopic series. It is also revealed that isotopes of Nb with mass number $A \sim 124$ in RMF, SHF and A=133 for Ag in FRDM are found to be most tightly bound nucleus for the considered drip-line nuclei. From the calculated binding energy, we estimated the one neutron separation energy S_n and predicted the neutron drip-line for *Cu — Sn.* Based on the information of S_n, drip-line and waiting point, a rapid neutron capture path is suggested for $Z = 29 — 50$. The prediction of the present *r*—process path may be a gate way for the formation of neutron-rich as well as superheavy nuclei.

6. ACKNOWLEDGMENTS

REFERENCES

[1] E. M. Burbidge, G. R. Burdige, W. A. Fowler and F. Hoyle, Rev. Mod. Phys. **29**, 547 (1957) http://dx.doi.org/10.1103/RevModPhys.29.547

[2] A. G. W. Cameron, Chalk River rep. no. CRL-41, Chalk River Labs. Chalk River, Ontario (1957)

[3] J. J. Cowan and F. -K. Thielemann Phys. Today (October) **47** (2004)

[4] Y. -Z. Qian and S. E. Woosley, Astrophys. J. 471, 331 (1996) http://dx.doi.org/10.1086/177973

[5] R. D. Hoffman, S. E. Woosley and Y. -Z. Qian, Astrophys. J. 482, 951 (1997) http://dx.doi.org/10.1086/304181

[6] K. Otsuki, H. Tagoshi, T. Kajino and S. Wanajo, Astrophys. J. 533, 424 (2000) http://dx.doi.org/10.1086/308632

[7] T. A. Thompson, A. Burrows and B. S. Meyer, Astrophys. J. 562, 887 (2001) http://dx.doi.org/10.1086/323861

[8] K. Langanke and J. Martinez-Pinedo, Rev. of Mod. Phys. **75**, 819 (2003) http://dx.doi.org/10.1103/RevModPhys.75.819

[9] J. J. Cowan, F. -K. Thielemann and J. W. Truran, Phys. Rep. 208, 267 (1991) http://dx.doi.org/10.1016/0370-1573(91)90070-3

[10] C. Sneden and J. J. Cowan, Science 299, 70 (2003) http://dx.doi.org/10.1126/science.1077506

[11] M. Arnould, S. Goriely and K. Takahashi, Phys. Repts. 450, 97 (2007) http://dx.doi.org/10.1016/j.physrep.2007.06.002

[12] H. Grawe, K. Langanke and G. Martnez-Pinedo, Rep. Prog. Phys. **70**, 1525 (2007) http://dx.doi.org/10.1088/0034-4885/70/9/R02

[13] S. K. Patra, R. K. Choudhury and L. Satpathy, J. Phys. G **37**, 085103 (2010) http://dx.doi.org/10.1088/0954-3899/37/8/085103

[14] L. Satpathy, S. K. Patra and R. K. Choudhury, PRAMANA - J. Phys. 70 87 (2008)

Ikram, M.
Singh, S.K.
Patra, S.K.

[15] P. Moller, J. R. Nix, W. D. Myers and W. J. Swiatecki, At. Data and Nucl. Data Tables **59**, 185 (1995) http://dx.doi.org/10.1006/adnd.1995.1002

[16] P. Moller, J. R. Nix and K. -L. Kratz, At. Data and Nucl. Data Tables 66, 131 (1997) http://dx.doi.org/10.1006/adnd.1997.0746

[17] J. Boguta and A. R. Bodmer, Nucl. Phys. A 292, 413 (1977) http://dx.doi.org/10.1016/0375-9474(77)90626-1

[18] B. D. Serot, Rep. Prog. Phys. **55**, 1855 (1992) http://dx.doi.org/10.1088/0034-4885/55/11/001

[19] Y. K. Gambhir, P. Ring and A. Thimet, Ann. Phys. (N.Y.) 198, 132 (1990) http://dx.doi.org/10.1016/0003-4916(90)90330-Q

[20] P. K. Panda, S. K. Patra, J. Reinhardt, J. A. Maruhn, H. Stocker and W. Greiner, Int. J. Mod. Phys. E 6, 307 (1997) http://dx.doi.org/10.1142/S0218301397000202

[21] G. A. Lalazissis, S. Karatzikos, R. Fossion, D. Pena Arteaga, A. V. Afanasjev and P. Ring, Physics Letters B 671, 36 (2009) http://dx.doi.org/10.1016/j.physletb.2008.11.070

[22] E. Chabanat, P. Bonche, P. Hansel, J. Mayer and R. Schaeffer, Nucl. Phys. A 627, 710 (1997). http://dx.doi.org/10.1016/S0375-9474(97)00596-4

[23] J. R. Stone and P. G. Reinhard, Prog. Part. Nucl. Phys. **58**, 587 (2007) http://dx.doi.org/10.1016/j.ppnp.2006.07.001

[24] P. -G. Reinhard and H. Flocard, Nucl. Phys. A 584, 467 (1995) http://dx.doi.org/10.1016/0375-9474(94)00770-N

[25] M. Wang, G. Audi, A.H. Wapstra, F.G. Kondev, M. MacCormick, X. Xu and B. Pfeiffer, Chinese Physics C **36**, 1603 (2012). http://dx.doi.org/10.1088/1674-1137/36/12/003

[26] R. Baruah, K. Duorah and H. L. Duorah, J. Astrophys. Astr. **30**, 165 (2009) http://dx.doi.org/10.1007/s12036-009-0013-x

[27] R. N. Panda and S. K. Patra, J. Mod. Phys. **1**, 312 (2010) http://dx.doi.org/10.4236/jmp.2010.15044

[28] C. Lahiri and G. Gangopadhyay, Int. J. Mod. Phys. E **21**, 1250042 (2012) http://dx.doi.org/10.1142/S0218301312500425